MULTISTABLE FABRY-PEROT RESONATOR WITH AN ACTIVE SAGNAC INTERFEROMETER AS ITS RETRO-REFLECTOR

Yao LI, George EICHMANN and R.R. ALFANO

Department of Electrical Engineering, and the Institute for Ultrafast Spectroscopy and Lasers, City College of The City University of New York, New York, NY 10031, USA

Received 7 July 1986; revised manuscript received 12 August 1986

Multistable operations of an active Fabry-Perot (FP) resonator with an active Sagnac interferometer as its optically pumped variable reflectance retro-reflector (SIFP), is analyzed. Intensity-dependent transmission (reflection) curves are derived. The corresponding multistable operation is also indicated. By adjusting the SIFP parameters, it can be configured to be either an optical limiter, or an amplifier, or a logic or a memory element.

1. Introduction

Recently, the dynamic properties of a Sagnac, also known as a cyclic or an antiresonant ring, interferometer (SI) have been studied. A passive SI is a highly mechanically autostabilized device [1] that can be used as an optical retro-reflector. Using the SI as an equivalent end reflector, both mode-locked Nd:glass and dye lasers have been constructed [2,3]. Among its applications are laser cavity dumping [4], optical nonlinear parameter measurements [5], optical switching [5,6], and optical digital computing [7].

To study optical multistability, there are two major analytic approaches. In the first approach, Maxwell's equations together with proper boundary conditions are utilized to analyze multistability in different optical resonator geometries, such as a co-linear Fabry-Perot (FP) resonator [8], a ring resonator [9], etc. In a second approach, introduced by Felber and Marburger (F-M) [10], a replacement of a linear by an equivalent nonlinear refractive index in a non-absorbing co-linear type FP resonator is used. In this work, the use of a FP resonator with an active SI as its retro-reflector (SIFP), is proposed. In the following sections, both passive SIFP transmission and reflection equations are derived. By substituting the linear by its nonlinear intensity-dependent phase counterpart and using the F-M approach, subsequently, different aspects of an active SIFP are studied. Finally, the use of an active SIFP to perform optical amplification, limiting, and digital logic are also described.

2. The SIFP as an equivalent FP cavity

In fig. 1(a), an SIFP with three mirrors ($M_i, i = 1,2,3$) and a beam-splitter (BS) and with wave direction-dependent amplitude transmission and reflection coefficients as $t_j(t_j')$ and $r_j(r_j')$ with $j = 1, b$, and with round-trip phases for the co-linear, the clockwise (counterclockwise) SI sections as δ_l, $\delta_{s1}(\delta_{s2})$, respectively, is depicted. In fig. 1(b), an equivalent FP for this SIFP is shown. The purpose of this section is to derive the intensity dependent transmission (reflection) coefficients of its equivalent FP.

The SI complex amplitude transmittance and reflectance, denoted as $\tilde{t}_s$ and $\tilde{r}_s$, are ‡

$$\tilde{t}_s = r_2 r_3 [t_b^2 \exp(i\Delta\delta_s/2) - r_b^2 \exp(-i\Delta\delta_s/2)] \exp(i\bar{\delta}_s) , \quad (1)$$

$$\tilde{r}_s = 2 r_2 r_3 r_b t_b \cos(\Delta\delta_s/2) \exp(i\bar{\delta}_s) , \quad (2)$$

where the average SI counterpropagating wave phase

‡ A similar equation has been described in ref. [1]. Here, we let two SI counterpropagating beams have different round-trip phases ($\delta_{s1} \neq \delta_{s2}$).

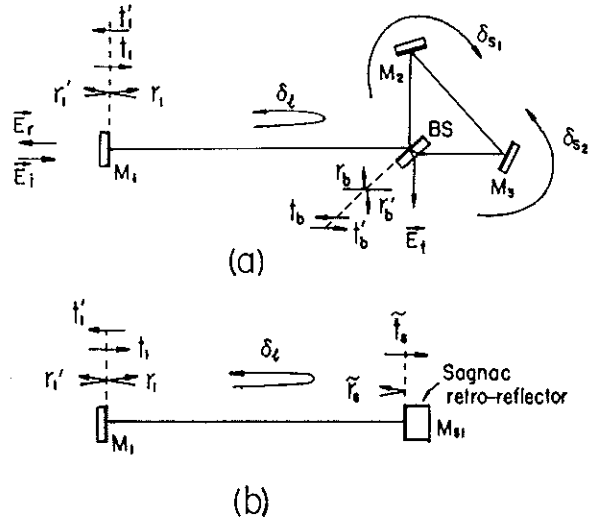

Fig. 1. (a) A schematic diagram of the SIFP: E_i and $E_t(E_r)$, the resonator input and transmitted (reflected) output waves: M_i ($i = 1, 2, 3$), mirrors: BS, beamsplitter; $t_i(t_i')$ and r_i' ($i = 1, b$), direction-dependent mirror and BS wave amplitude transmittance and reflectance; δ_l and δ_{s1} (δ_{s2}), co-linear section and the SI clockwise (counterclockwise) section round-trip phases. (b) The equivalent FP diagram with an effective SI as an retro-reflector (M_{SI}), $\tilde{t}_s$ and $\tilde{r}_s$, SI wave amplitude effective transmittance and reflectance.

and phase difference are $\bar{\delta} = (\delta_{s1} + \delta_{s2})/2$ and $\Delta\delta_s = \delta_{s1} - \delta_{s2}$, respectively. The corresponding SI intensity transmittance (T_s) and reflectance (R_s) are

$$T_s = |\tilde{t}_s|^2 = R_2R_3 - R_s\,, \tag{3}$$

$$R_s = |\tilde{r}_s|^2 = 4R_2R_3R_bT_b\cos^2(\Delta\delta_s/2)$$

$$= R_{sm}\cos^2(\Delta\delta_s/2)\,, \tag{4}$$

where R_{sm} is the maximum SI intensity reflectance. In agreement with ref. [1] for unity intensity reflectance for both R_2 and R_3 and $R_s = T_s = 0.5$. Eqs. (3) and (4) become zero and one, respectively.

For the SIFP, the equivalent amplitude transmission (t) and reflection (r) coefficients are

$$t = \frac{E_t}{E_i} = \frac{t_1\tilde{t}_s\exp(i\delta_l/2)}{1 - r_1\tilde{r}_s\exp(i\delta_l)}$$

$$r = \frac{E_r}{E_i} = \frac{r_1' + \tilde{r}_s\exp(i\delta_l)}{1 - r_1\tilde{r}_s\exp(i\delta_l)}\,. \tag{5}$$

Using eqs. (1)–(5), the SIFP intensity transmittance (T) and reflectance (R) are

$$T = |t|^2 = \frac{A}{1 + F\sin^2(\delta_T/2)}, \tag{6}$$

$$R = |r|^2 = \frac{B + F\sin^2(\delta_T/2)}{1 + F\sin^2(\delta_T/2)}, \tag{7}$$

where

$$F = \frac{4\sqrt{R_1R_s}}{(1 - \sqrt{R_1R_s})^2}, \tag{8}$$

$$A = \frac{(1 - R_1)(R_2R_3 - R_s)}{(1 - \sqrt{R_1R_s})^2}, \tag{9}$$

and

$$B = \left|\frac{\sqrt{R_1} - \sqrt{R_s}}{1 - \sqrt{R_1R_s}}\right|^2, \tag{10}$$

where the total round-trip phase is $\delta_T = (\delta_l + \bar{\delta}_s)$. For the SIFP, in addition to a total round-trip phase δ_T, because of the use of R_s, both T and R also depend on the SI beam counterpropagating phase difference $\Delta\delta_s$. Similar to an active FP, an intensity-dependent nonlinear refractive material (NLM) can be used to modulate both R_s and $T(R)$ leading to an intensity-dependent cavity round-trip phase. The intensity-dependent round-trip phase, in turn, changes the cavity transmittance (reflectance) and results in multistable behavior of the equivalent FP cavity.

3. Active SIFP

A passive SI is a mechanically stable device. However, the use of intensity dependent nonlinear materials within the SIFP can cause the device to be optically multistable. Since different NLM placements in a SIFP can cause completely different transmission (reflection) effects, two different cases need to be considered. First, let the averaged SI phase $\bar{\delta}_s$ be fixed while the co-linear section phase δ_l vary. Because now the two SI counterpropagating waves traverse identical optical path, the SI phase difference is

zero or $\delta_{s1} = \delta_{s2}$. Thus, from eq. (4), $R_s = R_{sm}$ is fixed. This is similar to a co-linear FP case. Since the parameters R_2 and R_3 are not always equal to unity, in eq. (9), instead of the usual co-linear factor $(1 - R_s)$ the factor $(R_2 R_3 - R_s)$ is used. This replacement causes the SIFP transmission modulation to be lower than that of the corresponding FP. For an equal-ratio BS, the power transmission of eqs. (6) and (9) reduces to zero, while for a non-equal-ratio BS, transmission (reflection) expressions are similar to a conventional FP expressions. Thus, further discussions on its characteristics are omitted.

Next, we let the co-linear phase δ_l be fixed while we vary, with the pump intensity, the average phase $\bar{\delta}_s$. Because the two SI counterpropagating beams now traverse different optical paths, the SI phase difference is nonzero. As the phase difference $\Delta\delta_s$ changes, R_s oscillates between its maximum value R_{sm} and zero. This configuration is equivalent to a co-linear FP with a single fixed and a variable reflectance mirror. By inserting a cubic optical NLM in the SI loop, i.e. $n = n_0 + n_2 \langle E^2 \rangle$, and using an non-equal-ratio BS, an intensity-dependent non-zero phase difference $\Delta\delta_s$ can be obtained [6,9]. Substituting in eqs. (6) and (7) the relations

$$\delta_T = \delta_{T0} + \Delta\bar{\delta}_s \,, \tag{11}$$

$$\Delta\delta_s = (2R_b - 1)\,\Delta\bar{\delta}_s$$

$$= (2R_b - 1)(2\pi L/\lambda)\, n_2 \langle E^2 \rangle \,, \tag{12}$$

where δ_{T0}, $\Delta\bar{\delta}_s$ and L are the initial total round-trip phase, the SI average phase change and the NLM cell length, respectively, results in an intensity-dependent SIFP transmission (reflection) curve. While with a FP tuning either the mirror reflectance or the initial resonator phase either affects the transmission modulation depth or translates the transmission curve, with a SIFP, because of different sine- and cosine-square function frequencies and initial phases in eqs. (4), (6) and (7),

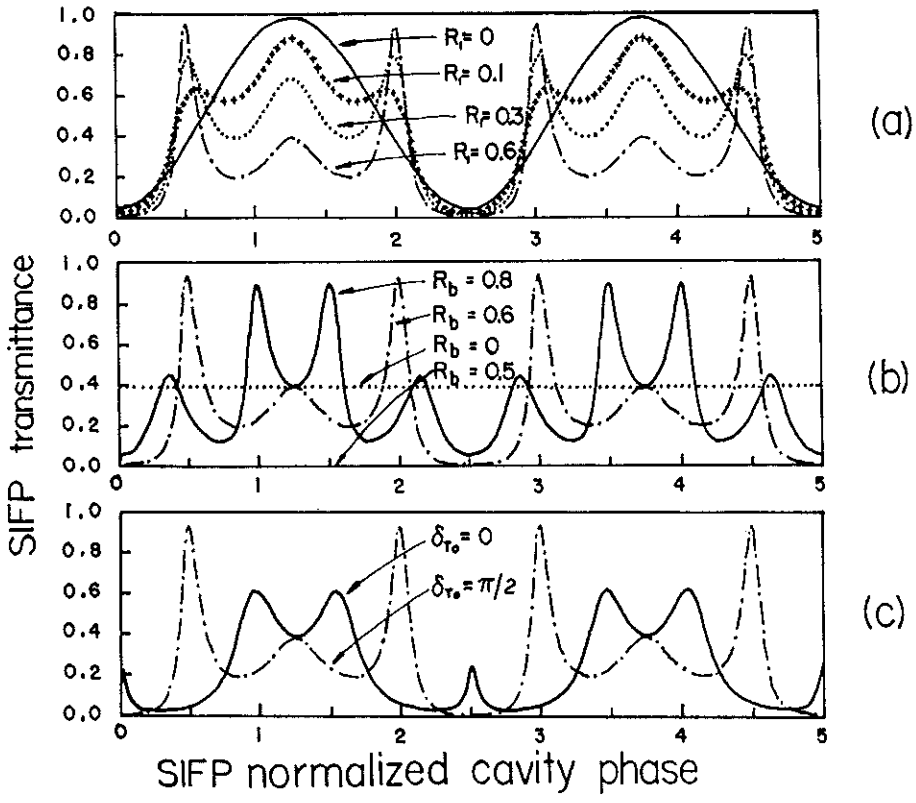

Fig. 2. Intensity transmission versus SIFP normalized resonator phase curves with adjustable parameters (a) input mirror reflectance R_1; (b) BS reflectance R_b and (c) resonator initial phase δ_{T0}.

the corresponding tuning can result in radically different curves.

As examples, in figs. 2(a, b, c), three sets of the SIFP transmission versus input intensity curves, with different adjustable parameters R_1, R_b and δ_{T0} are shown. In fig. 2(a), the effect of changing the front mirror reflectance R_1 is shown. For large R_1, because in each period the peaks of the two off-center resonances are higher than the center resonance peak there are two dominant transmission regions. These multiple resonances are due to competitions between different sine- and cosine-square phase functions. Also, because of multiple-beam interference, the resonance bands are relatively narrow. As R_1 decreases, the resonance curve broadens and the center (side) transmission gradually increases (decreases). As R_1 approaches zero, in agreement with ref. [6] the off-center peaks recede yielding a single SI sinusoidal transmission curve. By varying the BS reflectance R_b, the curves of fig. 2(b) are obtained. Two extreme cases, when R_b is equal to 0.0 (1.0) and 0.5 (a equal-ratio BS), are of interest. In the former case, a constant bias $(1-R_1)R_2R_3$ curve is obtained indicating, that in this case, there is no interference effect. For a balanced (equal-ratio) BS, because on both sides of the NLM the SI incident intensities are identical, the SI phase difference is zero and, therefore, $R_s = R_{sm}$ is fixed. Although the intensity-dependent round-trip SI phase $\bar{\delta}_s = \delta_{s1} = \delta_{s2}$ does vary, independent of δ_T, $(R_2R_3 - R_s)$ is always equal to zero. Thus, except for a change in geometry, the above two special cases belong to a FP category. In fig. 2(c), the effect of varying the initial phase δ_{T0} is illustrated. Unlike a FP, where a change of the initial phase translates the transmission curve, here, a change in the initial phase, because it only affects the sine-square function, modifies the transmission curve.

To study resonator multistability phenomena, the SIFP transmission (reflection) curves of fig. 2 are utilized. Using the F-M method, taking transmission as an example, eq. (6) is interpreted as a solution of two simultaneous equations where the left hand side is a linear equation with a fixed slope as a function of input intensity while the right hand side is the nonlinear intensity-dependent transmission curve [10]. For a given slope, wherever multiple intersections of two curves can be found, multistable intensity transmissions may exist. When a pump beam illuminated

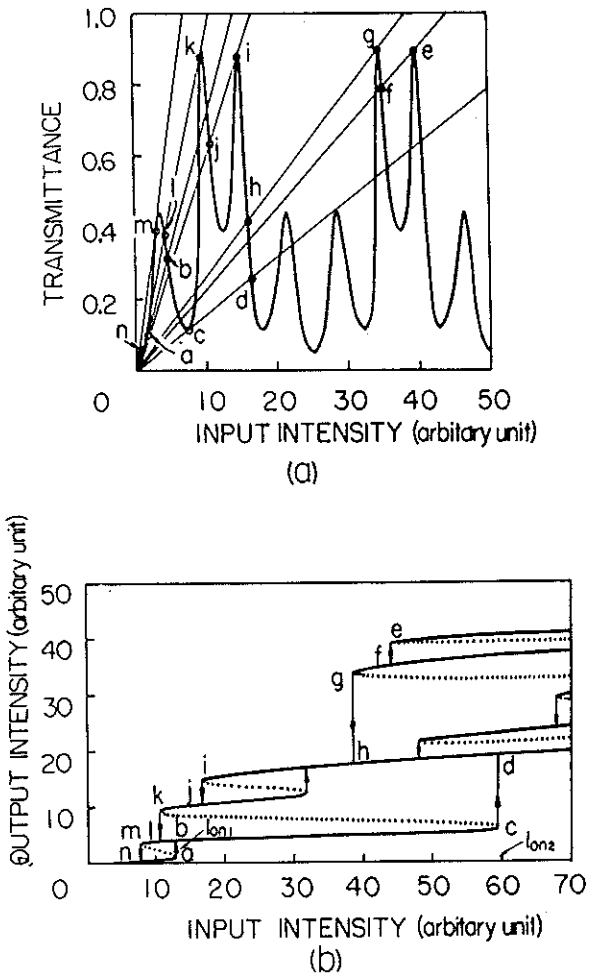

Fig. 3. (a) Typical SIFP transmission versus input intensity curve used for SIFP multistability analysis. Intersections of the straight line with the nonlinear transmission curve indicate multiple critical switching input and output intensities. (b) Multistable input and output SIFP intensity relations with corresponding critical switching points a, b through m, n.

co-linear section NLM is used, the corresponding multistable SIFP operators exhibits the same characteristics as does the usual co-linear FP. For this case both experimental and theoretical results are available [8,10,11]. When a pump beam illuminated SI section NLM is used, different multistable operation is expected. In fig. 3(a), indicated by the solid line, two cycles of a fig. 2(b) SIFP transmission curve is shown. The horizontal and vertical axes represent the input intensity and SIFP intensity transmittance, respectively. Initially, indicated by the intersection between

the transmission curve and the vertical coordinate, the SIFP is in a low transmission state. Increasing the input intensity decreases the slope of the straight-line. The intersection then gradually moves up toward a point a where the straight line is tangent to the nonlinear curve. Correspondingly, the output intensity slowly increases. By increasing the input intensity (a further decrease in the straight line slope), a second intersection between the straight line and the nonlinear curve is sought. The closest intersection to a is the point b which is the next transmission state. Increasing the input intensity until the intersection reaches another tangential point c results in a slowly increasing output intensity. Past intersection c, another sudden jump brings the transmission state to a new intersection d resulting in another output intensity jump. Similarly, by continuously decreasing the output intensity the intensity-dependent transmission is forced to change from point e through n, and finally reaches a zero output intensity state. In fig. 3(b) the corresponding multistable intensity discontinuities are illustrated. The first (second) switch-on threshold input intensities are labeled as $I_{on\,1}$ ($I_{on\,2}$), respectively. To obtain bistability, the input intensity should be below $I_{on\,2}$. For input intensities larger than $I_{on\,2}$, a number of output intensity levels can be probed. In principle, a SIFP and the nonlinear antiresonant ring interferometric switch proposed by ref. [6] have the same switching power requirement. In both devices, using an identical NLM, the switching power depends on the BS intensity transmittance (reflectance). The larger the imbalance between the values of the BS intensity transmittance and reflectance, the less the switching power is required. To lower the switching power requirement, materials with a large nonlinearity must be used. However, some large nonlinearity materials can have a severe carrier diffusion problem. For example, because the diffusion length is 60 μm in a InSb [12,13], nonlinear index modulation of a period less than this length will be washed out. To overcome the diffusion problem, the use of multiple-quantum-well semiconductor materials may be helpful [14]. It has been reported that semiconductor-doped glasses can produce large, fast and diffusion-free optical third order nonlinearities [15].

4. Applications

Finally, compared to a nonlinear FP, a nonlinear multistable SIFP is a flexible device with several additional adjustable parameters. The NLM may be placed in either one of two possible locations. With this device, in addition to the primary (cavity) input beam, using differently placed NLMs other external incident beams can also be used. As the overall inducing intensity exceeds the first switch-on threshold, both hysteretic and non-hysteretic bistabilities are obtainable. While a hysteretic bistability is suitable for optical memory and sequential logic operations, for asynchronous logic operation, a non-hysteretic bistability can be used to implement an optical limiter or a switch. The use of higher input intensities can cause SIFP multistable outputs. The tuning of initial phase, and other parameters such as BS reflectivity, can totally change the transmission curve. Properly choosing these parameters leads to different multistable operations. A SIFP multistability application is multistable optical switching. A combination of different SIFP multistable operation modes may help in the design of multiple-valued optical logic and arithmetic computing elements.

5. Summary

To summarize, nonlinear operations in a FP cavity consisting of a Sagnac interferometer and reflector are studied. A simple model that uses plane wave, and non-absorbing refractive nonlinearity assumptions is described. Different aspects of this active device are outlined. Applications in optical switching and computing are indicated.

Acknowledgement

Constructive comments by the referee are deeply appreciated. This work was supported in part by a grant from the Air Force Office of Scientific Research.

References

[1] A.E. Siegman, IEEE J. Quantum Electron. QE-9 (1973) 247.
[2] J.M. Buchert, D.K. Basa, C. Tzu and R.R. Alfano, J. Appl. Phys. 55 (1984) 683.
[3] H. Vanherzeele, R. Torti and J.-C. Diels, Appl. Optics 23 (1984) 4182.
[4] R. Trutna and A.E. Siegman, IEEE J. Quantum Electron. QE-13 (1977) 955.
[5] Y. Li, G. Eichmann and R.R. Alfano, Appl. Optics 209 (1986).
[6] K. Otsuka, Optics Lett. 8 (1983) 471.
[7] G. Eichmann, Y. Li and R.R. Alfano, Opt. Eng. 25 (1986) 91.
[8] D.A.B. Miller, IEEE J. Quantum Electron. QE-17 (1981) 306.
[9] A.E. Kaplan and P. Meystre, Optics Comm. 40 (1982) 229.
[10] F.S. Felber and J.M. Marburger, Appl. Phys. Lett. 28 (1976) 731.
[11] S.D. Smith, A.C. Walker, B.S. Wherrett, F.A.P. Tooley, J.G.H. Mathew, M.R. Taghizadeh and I. Janossy, Appl. Optics 25 (1986) 1586.
[12] H.A. MacKenzie, D.J. Hagan and H.A. Al-Attar, Optics Comm. 51 (1984) 352.
[13] D.J. Hagan, H.A. MacKenzie, H.A. Al-Attar and W.J. Firth, Optics Lett. 10 (1985) 187.
[14] D.A.B. Miller, D.S. Chemla, D.J. Eilenberger, P.W. Smith, A.C. Gossard and W.T. Tsang, Appl. Phys. Lett. 41 (1982) 679.
[15] S.S. Yao, C. Karaguleff, A. Gabel, R. Fortenberry, C.T. Seaton and G.I. Stegeman, Appl. Phys. Lett. 46 (1985) 801.